Mantle Anchor Structure: An argument for bottom up tectonics

Adam M. Dziewonski [a,*], Vedran Lekic [b,1], Barbara A. Romanowicz [b]

[a] Department of Earth and Planetary Sciences, Harvard University, Cambridge, MA, USA
[b] Berkeley Seismological Laboratory, University of California, Berkeley, CA, USA

ARTICLE INFO

ABSTRACT

Close examination of the long wavelength shear velocity signal in the lowermost mantle in the wavenumber domain ties several geophysical observations together and leads to fundamental inferences. When mantle shear velocity model S362ANI at a depth of 2800 km is expanded in spherical harmonics up to degree 18, more than one half of the seismic model's total power is contained in a single spherical harmonic coefficient: the "recumbent" Y_{20} spherical harmonic; a Y_{20} with its axis of symmetry rotated to the equatorial plane. This degree 2 signal, which continues with decreasing amplitude for more than 1000 km above the core–mantle boundary (CMB), is characterized by two antipodal regions of low velocities, separated by a circum-polar torus of higher than average velocities. If the slow regions are associated with net excess mass, then any axis of rotation located in the plane of the circum-polar torus will be close to the maximum moment of inertia axis; this includes, of course, the current axis of rotation. We suggest that the recumbent Y_{20} is a very stable feature: once established, it is difficult to erase, and only relatively small departures from this equilibrium configuration are possible. This anomaly correlates strongly with the degree 2 terms of the residual geoid expansion, distribution of the hot spots above the slow regions, high attenuation in the transition zone, and position of subduction zones above the fast band during the last 200 Ma. Also, the preferred paths of the virtual geomagnetic pole and true polar wander locations for the last 200 Ma lie within the fast band. Since the non-hydrostatic perturbation of the moment of inertia tensor depends only on degree-2 anomalies in the density distribution and deformation of discontinuities, it is natural to infer that rotational dynamics of the Earth have influenced the distribution of heterogeneities in the Earth's deep interior. We propose that the large-scale heterogeneity at the base of the mantle, which we name Mantle Anchor Structure (MAS) may have formed early in the history of the convecting mantle, remained locked in place with respect to the Earth's rotation axis ever since, and is currently imposing the planform of flow in the mantle and of plate tectonics at the surface.

© 2010 Elsevier B.V. All rights reserved.

1. Introduction

The motivation for the first attempt to map seismic velocity anomalies in three dimensions on the global scale (Dziewonski et al., 1977) was to identify the driving mechanism of plate tectonics. Even this initial, very low resolution study detected significant correlation between degree 2 and 3 velocity anomalies in the lowermost mantle and the corresponding geoid coefficients, demonstrating the capability of the tomographic approach to resolve an otherwise nonunique inverse problem. Furthermore, that study, as well as that of Masters et al. (1982), motivated Busse (1983) to propose a degree-2 (quadrupole) layered convection in the mantle with the lower mantle pattern being that of the "recumbent" Y_{20}, even though this pattern was not that clear in the seismic models available then; Busse has also suggested that this pattern could be very stable.

Le Pichon and Huchon (1984) reached a similar conclusion, and pointed out the correspondence of geoid lows with subduction and geoid highs with the seafloor spreading. Cazenave et al. (1989) pointed out the correlation at degree-2 of regions of elevated surface topography, geoid highs, low seismic velocities and the hotspot distribution.

Some correlations between geodynamic observables were noted even without tomographic information. For example, Crough and Jurdy (1980) note the correlation between the distribution of hotspots and the geoid corrected for the effect of slab subduction. Improved seismic models (Dziewonski, 1984; Woodhouse and Dziewonski, 1984) stimulated geodynamic research on the quasi-static response of a viscous Earth to internal loads in order to elucidate the relationship between velocity anomalies and the geoid (Forte and Peltier, 1987; Hager, 1984; Richards and Hager, 1984). The main objective was to determine the variation of viscosity with depth, although there is another unknown radial function involved: the coefficient of proportionality of velocity and density variations. There are tradeoffs, but the need for an increase in viscosity in the lower mantle by a factor

---

* Corresponding author.
  E-mail address: dziewons@eps.harvard.edu (A.M. Dziewonski).
[1] Now at: Department of Geological Sciences, Brown University, Providence, RI, USA.

between 10 and 100 times over that in the upper mantle seems to be robust. In general, these studies did not investigate how the seismic anomalies originated; for a detailed review, see Forte (2007).

Richards and Engebretson (1992) demonstrated that the geographical distribution of the mass of slabs subducted during the last 200 Ma agrees, for spherical harmonic coefficients of degrees 2 and 3, with the geoid signal, seismic velocities and hot spot distribution. This study was extended by Ricard et al. (1993), who reconstructed the history of subduction during the Cenozoic and Mesozoic periods, and, assuming that slabs sink vertically with imposed velocities, calculated the present day 3-D model of mass anomalies in the mantle. They found good agreement between a geoid computed for this model and the observed one. However, if this model was correct, then assuming a proportionality between density and velocity anomalies, it should predict travel time anomalies of phases such as *S* or *ScS*; regardless of the selection of the coefficient of proportionality, the pattern of the predicted and observed *ScS* residuals was entirely different (Guy Masters, personal communications). The sinking slab model was further developed by Lithgow-Bertelloni and Richards (1998) and we shall be using their slab model represented by a spherical harmonic expansion of density anomalies in 20 layers, spanning the depth range from Moho to CMB; we shall refer to this model as L-B&R.

The popularity of the sinking slab model was enhanced by images of unimpeded penetration of slabs into the lower mantle (Grand et al., 1997; van der Hilst et al., 1997). As a result, this slab-centric conceptual model has been widely accepted in the Earth Science community in the late 1990s. There were, however, serious reasons to doubt its completeness. The foremost was the absence of the intense, large-scale anomalies associated with the low velocity regions: the so-called African and Pacific Superplumes (Dziewonski et al., 1991, 1993) and more recently Large Low Shear Velocity Provinces, LLSVP (Garnero and McNamara, 2008). The other was that many of the slabs seemed to become stagnant in the upper mantle, or to stop at the depth of about 1000 km (Fukao et al., 2001) and that the global spectrum of lateral heterogeneity changed dramatically across the 650 km discontinuity (Gu et al., 2001; Ritsema et al., 2004).

Forte et al. (2002) have modeled mantle convection using as starting point density anomalies inferred from a tomographic study; they observed that the strong degree-2 pattern remained stable over a billion years. Some recent convection models (Bull et al., 2009; Foley and Becker, 2009; Zhong et al., 2007) match the redness of the spectrum in the lower mantle, but they do not capture the very particular distribution of anomalies observed seismically in the lowermost mantle, as well as the inferred stability in time. In a very recent paper, Zhang et al. (2010) present mantle convection calculations for the last 600 Ma which indicate that the Pacific and African superplumes changed their size and position during that time, but end with a thermal structure similar to that seen in the velocity anomalies near the CMB. On the other hand, the fixity of hotspots (Morgan, 1972) and the correlation of their long-wavelength distribution with the LLSVP prompted Davaille (1999) and Jellinek and Manga (2004) to experimentally study the relationship of large upwellings and plumes, of which hotspots may be the surface expression. In particular, Jellinek and Manga (2004) show how plumes originating in the deep mantle can cluster and be stabilized within major upwellings under specific composition, density and viscosity conditions.

Expanding data sets, improved model parameterizations, and more sophisticated modeling procedures have contributed to significant progress in tomographic studies of the mantle. In general, 3D models of shear velocity are better constrained than those of compressional velocity because surface waves, which control the upper mantle structure, are dominated by shear energy. There is, also, remarkable agreement among models obtained by different (not all) research groups (see, e.g. Becker and Boschi, 2002); this is particularly true of the models obtained using combined subsets of data that have good resolving power at all depths within the mantle.

In what follows, we summarize the seismic constraints on the pattern of heterogeneity, discuss their probable relation to the non-hydrostatic moment of inertia tensor and compare them with the predictions of the L-B&R model, separate radial correlation functions for the slow and fast velocity anomalies as well as the distribution of hotspots. We then draw conclusions from these comparisons and outline future directions of research necessary to explain the dynamic behavior of the Earth on a planetary scale. Some of our inferences have been made previously by various authors, who are credited with citations. The synthesis presented here leads us to the suggestion that the giant degree 2 anomaly imposes control on mantle circulation and is very long-lived; this is novel and may lead to new efforts to improve our understanding of the Earth's dynamics.
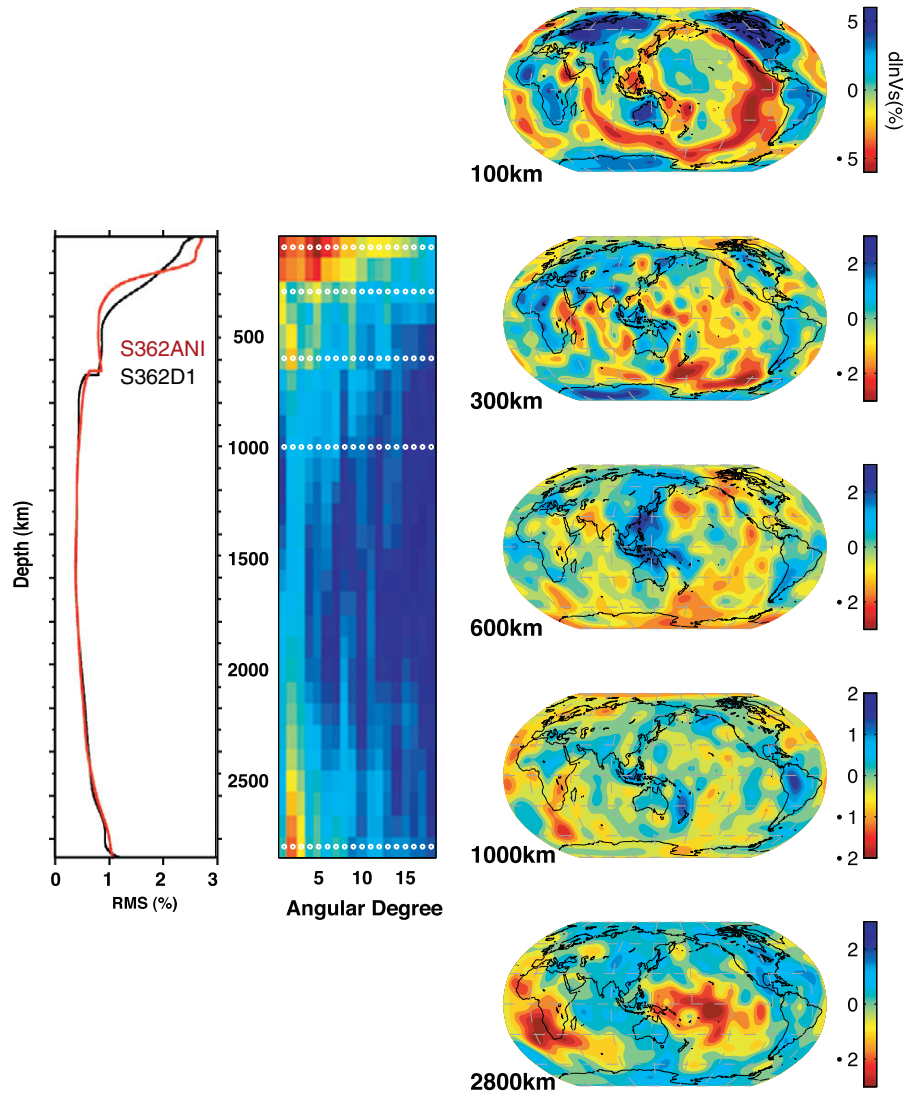
Even though we focus here on the very large wavelength component of the seismic model, there is copious evidence for the existence of shorter wavelength anomalies, particularly at the bottom of the mantle (for a review, see Lay, 2007). These may or may not be a part of this super-long wavelength dynamics; for example, Hartlep et al. (2003) present a model of convection in which large and small-scale flows can be separated by a gap in the power spectrum.

2. Seismic constraints

Global models of mantle shear velocity anomalies have reached "maturity". This does not mean that all structures of potential interest have been resolved; for this we do not have sufficient data coverage. Rather, it means that we have resolved, on the global scale, the dominant large-wavelength anomalies, because of the red nature of the power spectrum. In practice, this means that truncation of the spectrum at a range of order numbers at which the spectral power is rapidly decreasing does not alias the long-wavelength image of heterogeneities in the space domain significantly.

By "maturity" we also mean that all global 3D models of S-velocity anomalies obtained with data sets allowing good control over the structure from the top to the bottom of the mantle (i.e. including body wave and overtone data) show very similar features (Gu et al., 2001; Kustowski et al., 2008; Masters et al., 2000; Mégnin and Romanowicz, 2000; Panning and Romanowicz, 2006; Ritsema et al., 1999, which from here on will be referred to as KED). We shall use here S362ANI of KED as representative of this class of models; we refer the reader to Figures 8 and 9 in KED and Figures 4.7, 4.10–15 and 4.17–18 in Kustowski (2007) for direct comparison with other models. Specifically, the longest wavelength structure is nearly identical between the cited models. The advantage of global models is that they and their properties, such as power spectra, reflect the behavior of the system as a whole, rather than selected regions such as velocity anomalies near subduction zones; a spectrum of velocity anomalies also takes into account the vast areas away from subduction zones.

Figure 1 shows the r.m.s. amplitude of the isotropic part of model S362ANI compared to S362D1 (Gu et al., 2001) as a function of depth, power spectrum of the isotropic part of model S362ANI as a function of depth and harmonic degree, and horizontal slices through the model at five different depths. The intervals in which the power is high are seen at 100 km depth, 600 km depth and 2800 km depth; they are separated by regions of low amplitude, white spectrum. The near surface features are well understood: they are dominated by surface tectonics with very slow mid-ocean ridges, faster old oceans and very fast continental cratons and platforms. The maximum spectral power is at degree 5 and begins to decrease rapidly after degree 6. The r.m.s. of the model decreases threefold between 200 and 250 km depth range; this may be contrasted with a smoothly changing r.m.s. curve for an earlier model, S362D1 (Gu et al., 2001). The additional data and less radial smoothing explain the higher radial resolution of KED. This depth range contains both lithosphere and asthenosphere, yet has a unique signature in terms of the level of heterogeneity; we propose a new term "heterosphere" to indicate the

Fig. 1. *Left*: the r.m.s. of two mantle models; note the difference in the steep decrease of the r.m.s. in model S362ANI (red) with the largest gradient at about 225 km depth as compared to an earlier model S362D1 of Gu et al. (2001), in which the r.m.s. decreases gradually through upper mantle. We attribute this difference to an increase of the data set used to derive the model and weaker radial damping. *Center:* the power spectrum (logarithmic scale) of shear velocity anomalies as a function of harmonic order and depth for the model S362ANI. *Right:* the five maps show shear wave speed anomalies (in percent with respect to the mean at each depth) at 100, 300, 600, 1000 and 2800 km depth (marked by circles in the power spectrum plot). Note that the length scale of velocity anomalies varies among the individual maps; the map at 2800 km depth is dominated by very large wavelength features—their significance is the focal point of this paper.

properties of this region. At a depth of 300 km this clear association with the surface tectonics nearly vanishes. There is an intermittent occurrence of fast velocities coincident with subducted slabs and the average sub-continental structure is somewhat faster than sub-oceanic, but without a clear age signature.

The spectrum changes again in the transition zone, where the degree-2 signal is dominant and it appears to be associated with the wide high-velocity anomalies in the western Pacific and weaker ones under South America and South Atlantic. This can be interpreted as the ponding of the subducted slabs, also imaged in the space domain in regional and global studies (Fukao et al., 2001; Gu et al., 2001, 2003; van der Hilst et al., 1991); the latter paper demonstrates that these areas of fast velocities coincide with large wavelength depressions of the 650 km discontinuity.

The map at the top of the lower mantle (1000 km depth) is very different from that in the transition zone. The r.m.s. amplitude is lower, the spectrum is whiter and there is little continuity with the anomalies just above the 650 km discontinuity. There are three distinct high-velocity anomalies in the vicinity of deep slab subduction: Java, Tonga-Fiji and central South America. They may represent

local penetration of the subducted material into the lower mantle; in the Tonga-Fiji area, Pysklywec et al. (2003) associated it with a regional avalanche of slabs accumulated in the transition zone. The sharp change of the pattern of velocity anomalies associated with either thermal or compositional heterogeneities implies a significant reorganization of the mantle flow across the 650 km discontinuity (Gu et al., 2001; Ritsema et al., 2004; Woodward et al., 1994, KED). The disruption of flow at the 650 km discontinuity makes it more likely for a part of the subducted material to be recirculated in the upper mantle (Gonnermann and Mukhopadhyay, 2009). The spectrum in the mid-mantle is flat, the amplitudes are low and cross-correlations among various models are the poorest in this depth range. Even though the spectrum is relatively white, degree 2 remains the strongest, particularly in the model of Ritsema et al. (2004).

The anomalies increase in amplitude below 1800–2000 km depth and the maximum power shifts distinctly to degree 2. The amplitudes are the largest near the CMB, dominated by two large low shear velocity provinces centered beneath Africa and the Pacific, and surrounded by a circum-polar band of fast velocities. This pattern remains the same in the deepest 800–1000 km of the mantle; thus it

cannot be due only to the anomalous properties of the D″ region or post-perovskite phase change. There does not seem to be a discontinuous termination of the top of the lowermost mantle structure (Gu et al., 2001).

3. The anatomy of degree 2 anomalies in the lowermost mantle

The excess ellipticity of the geoid has been interpreted by MacDonald (1965) and McKenzie (1966) as a "fossil bulge": a remainder from the time when the Earth rotated more rapidly and had higher ellipticity. The geophysical consequence of this interpretation is an extremely high viscosity of the lower mantle; so high that convection in that region would be impossible. Goldreich and Toomre (1969) have shown, however, that the C_{20} coefficient of the geoid is comparable in value to the S_{22} and C_{22} coefficients and should be interpreted as an expression of density heterogeneity in the Earth's interior. If a three-dimensional density distribution $\delta\rho(r,\theta,\varphi)$ is expanded in spherical harmonics, only degree 0 and 2 coefficients contribute to the elements of the moment of inertia tensor; this is why the high power in degree 2 is so important.

The high power in degree 2 at the bottom of the mantle can be seen in Figure 1, but the logarithmic scale makes difficult a quantitative assessment of its importance. In Figure 2 we show the power in individual degrees for the velocity anomalies at 2800 km depth as well as the cumulative power integrated from degrees 1 to 18. The cumulative power graph shows that more than 50% of the total power is contained in degree 2; predominance of this degree requires detailed examination. *Note: our power spectrum is the sum of all the squared spherical harmonic coefficients (Su and Dziewonski, 1992) for a given degree l; in some studies (c.f. Becker and Boschi, 2002) this sum is divided by 2l + 1, making the spectrum look even more red.*

Figure 3 compares degree 2 velocity anomalies at a depth of 2800 km for three shear velocity models: S362ANI (KED), SAW24B16 (Megnin and Romanowicz, 2000) and S20RTS (Ritsema et al., 2004). The distribution of the anomalies is practically identical for all models. At degree 2, the two low velocity regions are centered on the equator and are separated by a circum-polar band of velocities higher than average and constant with latitude in the middle of the belt. Such a distribution corresponds to the coefficients C_{21} and S_{21} equal to zero and $(C_{22}^2 + S_{22}^2)^{1/2} = |C_{20}|$; this combination of the coefficients is the same as for the Y_{20} harmonic with its axis of symmetry in the equatorial plane: a "recumbent Y_{20}". In this coordinate system, the power in a single coefficient exceeds the total power in 359 coefficients. Such concentration of power can hardly be accidental; experiments with generating randomly five possible degree 2 coefficients show that the probability of obtaining a configuration such as shown in Figure 3 is less than 0.001. Assuming the life-time of a degree 2 structure to be on the order of 100 Ma, a structure such as

in Figure 3 should occur once in 100 Ga, or more than 20 times the age of the Earth; this does not include additionally low probability of an "accidental" accumulation of power in degree 2 as compared to other degrees. Interestingly, the pattern in Figure 3 is the same as in the mantle convection model proposed by Busse (1983; Fig. 1).

If the seismically slow regions represent a net mass excess (this may include the effect of dynamic deformation of discontinuity topography; see Forte et al., 1995), the current axis of rotation corresponds—as it must—to the maximum moment of inertia. However, any axis in the circum-polar plane is the maximum moment of inertia axis: this means that the true polar wander (TPW) due to redistribution of the mass within the Earth's interior (Steinberger and O'Connell, 1997) would be the most noticeable if a mass redistribution occurred within the fast velocity band. Figure 3 shows TPW poles determined by Besse and Courtillot (2002) for the last 200 Ma and, indeed, they are in the middle of the fast band. As we shall show later, this band corresponds to the degree 2 expansion of the cumulative mass of slabs subducted during the last 110 Ma. Note that Steinberger and Torsvik (2008) computed continental motion and rotation through time in a paleomagnetic reference frame and concluded to the long-term stability of the degree-two geoid and related mantle structure for at least the last 320 Ma.

Another inference is that the primary contribution to the non-hydrostatic moment of inertia tensor is controlled by the anomalies in the lowermost 1000 km of the mantle. These results and considerations lead us to the formulation of the primary hypothesis of this paper that the degree 2 velocity (and density) anomalies in the bottom 1000 km of the mantle represent a very long-lived feature, conceivably reaching back to the time of differentiation and solidification of the Earth. Further considerations will present an implication that this recumbent Y_{20} structure, which we call Mantle Anchor Structure (MAS), imposes the overall planform for surface tectonics.

4. Comparison of a seismic model with a sinking slab model

The L-B&R model specifies density anomalies in different depth ranges; we integrate these data over depth to represent the mass input at the Earth's surface for two time intervals: one for the last 15 Ma, representing the mass of slabs in the upper mantle, and the other at 110 Ma, which is representative of the surficial distribution of the mass of slabs subducted during that period; for brevity, we call these results SLAB15 and SLAB110. We shall compare these maps with those for the model S362ANI at 600 km depth and at 2800 km depth.

Figure 4 (left) shows power spectra of two seismic models S362ANI and SAW24B16 at 600 km depth with the spectrum of SLAB15 as well as degree-by-degree correlation between the seismic models and SLAB15 (right). Both seismic models have a distinct peak
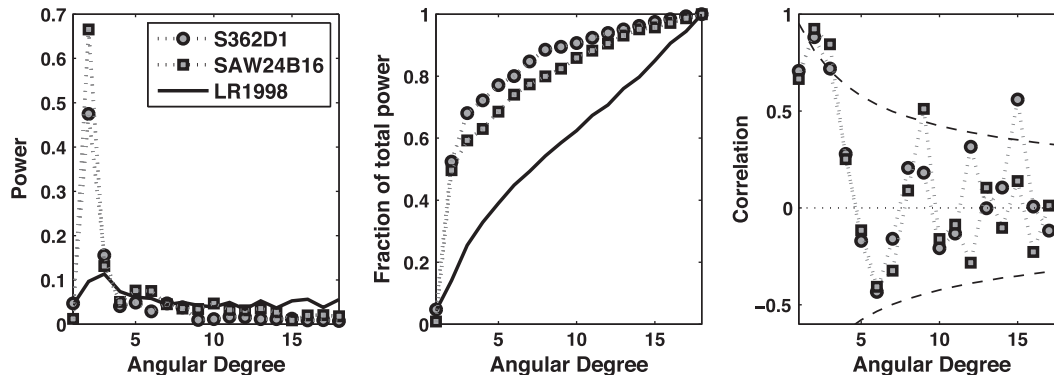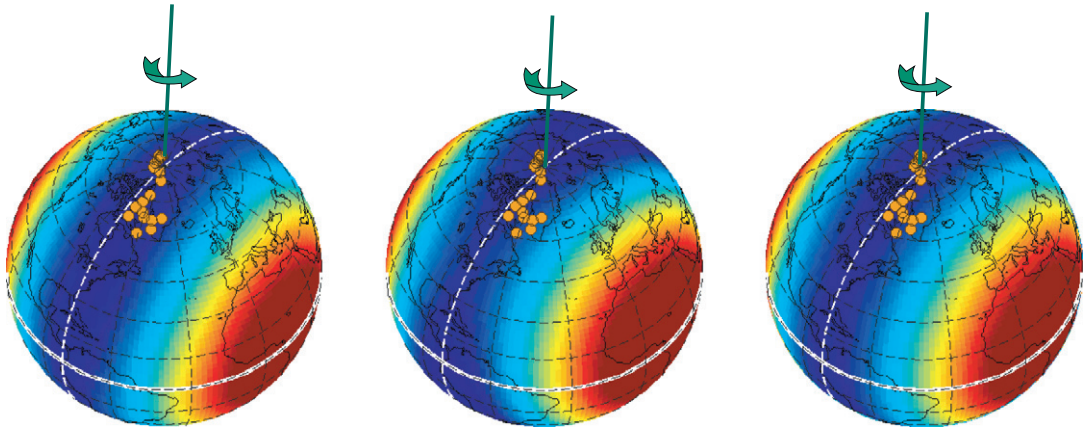

Fig. 2. *Left*: power spectra of S362ANI, SAW24B16 at 2800 km and the integrated mass anomaly of model L-B&R. *Center*: cumulative power spectra of the models. *Right*: correlations between each seismic model and the slab model as a function of angular degree. The dashed lines indicate 95% confidence level; this figure is further discussed in Section 4.

Fig. 3. The nearly-indistinguishable degree 2 structures at 2800 km depth of three global tomographic S-velocity models: (a) S362ANI; (b) SAW24B16; and (c) S20RTS. Pink circles indicate paleo-pole locations from the true polar wander reconstructions of Besse and Courtillot (2002).

at degree 2, while the SLAB15 spectrum is rather flat; this property is also reflected in the graph of cumulative power (middle), which increases more rapidly for the seismic models than for slabs. Statistically significant correlation occurs only for degree 2.
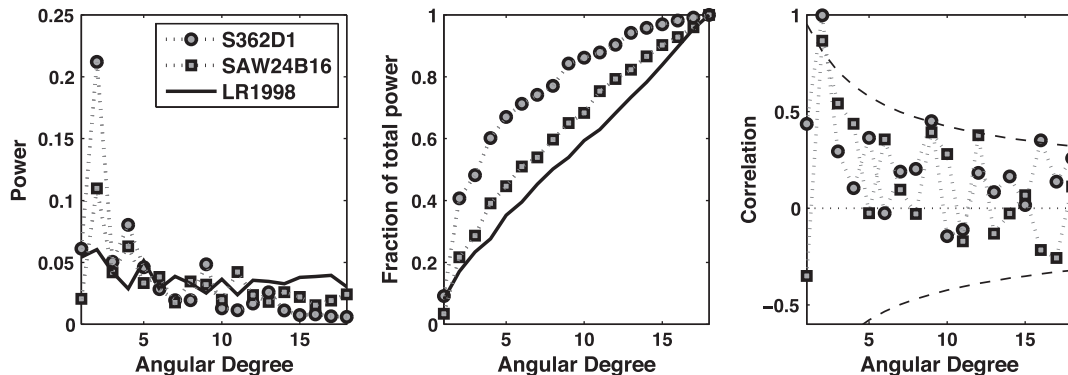
Figure 5 shows a comparison of the seismic model S362ANI with the SLAB15 model. The upper left panel shows S362ANI synthesized using harmonics from 1 to 18 at 600 km depth; whereas the upper right panel is the same for SLAB15 (the scale is arbitrary). The two maps have clearly different spectral contents; the anomalies in SLAB15, associated with the recent subduction, show a local maximum in the western Pacific and a weaker one under South America. Velocity anomalies attain maximum positive values in the same regions, but are much broader; there are also areas of negative velocity anomalies that do not have corresponding features in the SLAB15 map. The bottom row of Figure 5 shows the degree 2 components of S362ANI and SLAB15; the maps are essentially identical (correlation coefficient of 0.999), except for an arbitrary scaling factor. It is clear from comparison of this degree 2 structure to the maps for all degrees that the velocity anomalies in the transition zone correspond to the relatively large rate of subduction in the western Pacific and, to a lesser extent, under South America.

The implication of the similarity of the degree 2 patterns, as compared to the maps for all degrees, is that the interaction of the subducted slabs with the 650 km discontinuity fundamentally changes the spectral distribution of the subduction flux. The slabs, at least their majority, do not readily penetrate the 650 km discontinuity with only a decrease in their sinking rate, as the L-B&R model assumes, but they pond within the transition zone (TZ), as indicated by the velocity anomalies. In addition to other aspects of the TZ analysis, it is important because we can track the slabs from the surface to the transition zone using either seismic tomography or seismicity, providing a direct causal relationship between velocity and density anomalies.

What happens next to the ponded slabs cannot be readily inferred from seismological models; the latter are present time snapshots with the data used to derive them representing the state of the mantle during the last 15 years, on average. The "avalanche" model (Machetel and Weber, 1991; Solheim and Peltier, 1994; Tackley et al., 1993, 1994), in which material ponds above the endothermic phase change boundary, provides a mechanism needed to alter the spectrum of heterogeneity in a fashion similar to that inferred here. The location of large-scale velocity anomalies in the TZ correlates well with the topography of the 650 km discontinuity and the TZ thickness (Flanagan and Shearer, 1998; Gu et al., 2001, 2003), which is consistent with the ponded slabs representing a negatively buoyant, colder material. The other argument in favor of the resistance at the 650 km discontinuity comes from deep earthquakes in the transition zone offset 200–300 km away from the Wadati–Benioff zones (Lundgren and Giardini, 1994), as well as the change in the source mechanism of earthquakes in the deepest part of the subducted slab (Lekic, 2004).

Tracing of the flow below the transition zone is less straightforward. Figure 6 shows the radial correlation matrices (Jordan et al., 1993), whose elements contain correlation coefficients between velocity structures at two different depths; the diagonal elements are unity, by definition. The width of the band near the diagonal

Fig. 4. *Left:* power spectra of S362ANI and SAW24B16 at 600 km and the integrated upper mantle mass anomaly of model L-B&R. *Center:* cumulative power spectra. *Right:* correlations between each seismic model and the slab model as a function of angular degree. The dashed lines indicate 95% confidence level.
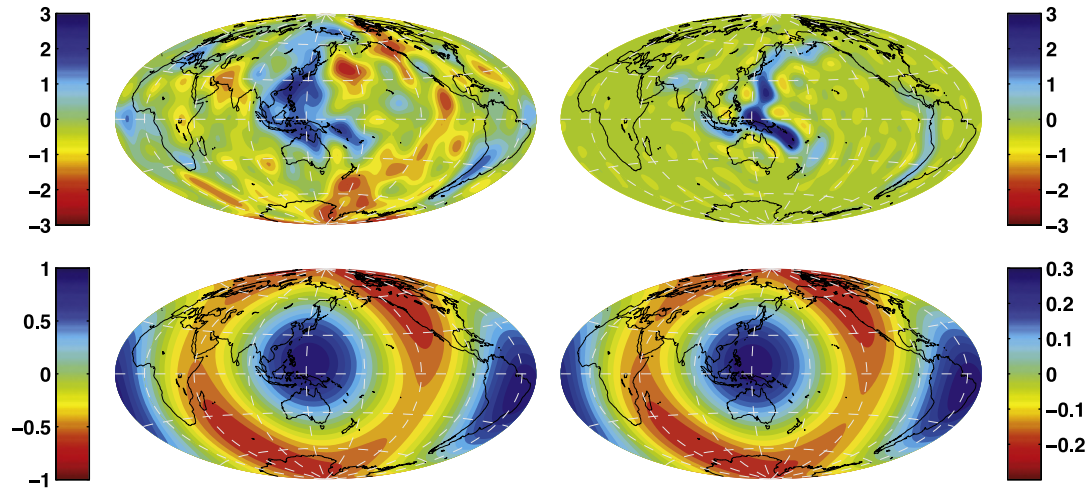
Fig. 5. *Left column:* comparison of seismic model S362ANI at 600 km and (*right column*) integrated mass anomaly for slab model L-B&R. The top maps show the velocity model at 600 km and the whole-mantle integrated slab model for degrees 1–18. The bottom row shows degree-2 pattern only (note the changed color scale).

region depends on the radial resolution of the data set, parameterization of the model and, what is most important, on the rate with which the actual structure changes in the radial direction. The specific parameterization used and resolution of the data sets indicate a resolving half-width of about 150 km in the lower mantle; in the

upper mantle, it may be as narrow as 50–75 km. Correlations outside that band indicate actual similarity, or dissimilarity, of the model at different depths. Usually, radial correlation matrices are computed for an entire model; here, we attempt to distinguish between radial correlations of fast and slow anomalies.

Figure 6 (top) shows the radial correlation function for slow anomalies (slower than −0.6% with respect to the mean at each depth). Note that slow anomalies correlate strongly (>0.5) across ~1000 km depth ranges. The other part of Figure 6 (bottom left) shows radial correlation function for the fast anomalies (faster than +0.6% with respect to the mean at each depth). Note that fast anomalies only correlate strongly (>0.5) across ~500 km depth ranges. We infer that slow anomalies are more continuous, while the fast anomalies (presumably representing sinking remnants of slabs) appear to be fragmented. This experiment tends to lend support to the avalanche hypothesis, even though they may represent a "drip" of the ponded slabs rather than complete flushing, as in Tackley et al. (1993). This is also seen in Figure 7 which represents a 3-D image of the lower mantle part of model S20RTS (Ritsema et al., 1999) filtered to degree 6 and truncated at 800 km depth to avoid obscuring the image by strong anomalies near the surface. The two columnar structures that emerge from the LLSVPs reach up to the bottom of the TZ.
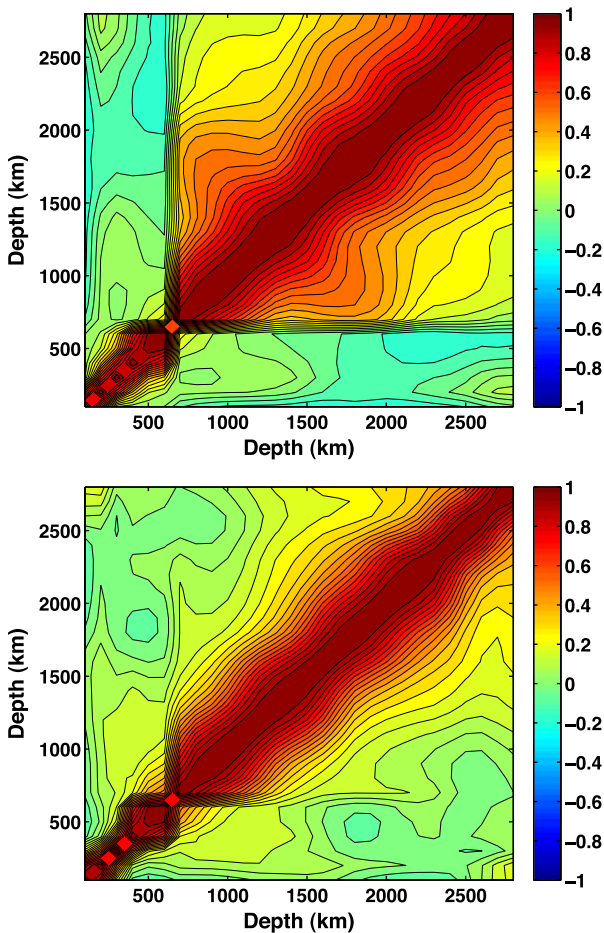

Fig. 6. Radial correlation functions (Jordan et al., 1993) of the model S362ANI. *Top*: only anomalies slower than average; *bottom*: only faster than average anomalies. Note that the slow anomalies have nearly twice the radial correlation length of the fast anomalies. This indicates that fast anomalies may be more fragmented.
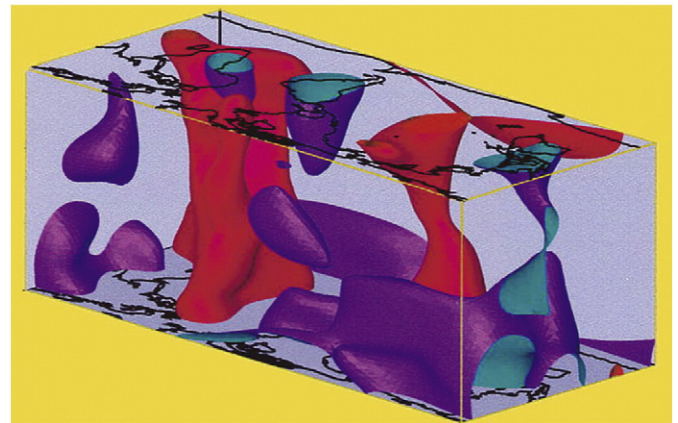

Fig. 7. Three dimensional view of model S20RTS filtered to degree 6. The red anomalies represent −0.6% iso-surfaces; blue anomalies show +0.6% iso-surfaces. Note that slow anomalies are continuous and form two pillars that reach to the transition zone; fast anomalies are more fragmented, except at the bottom.
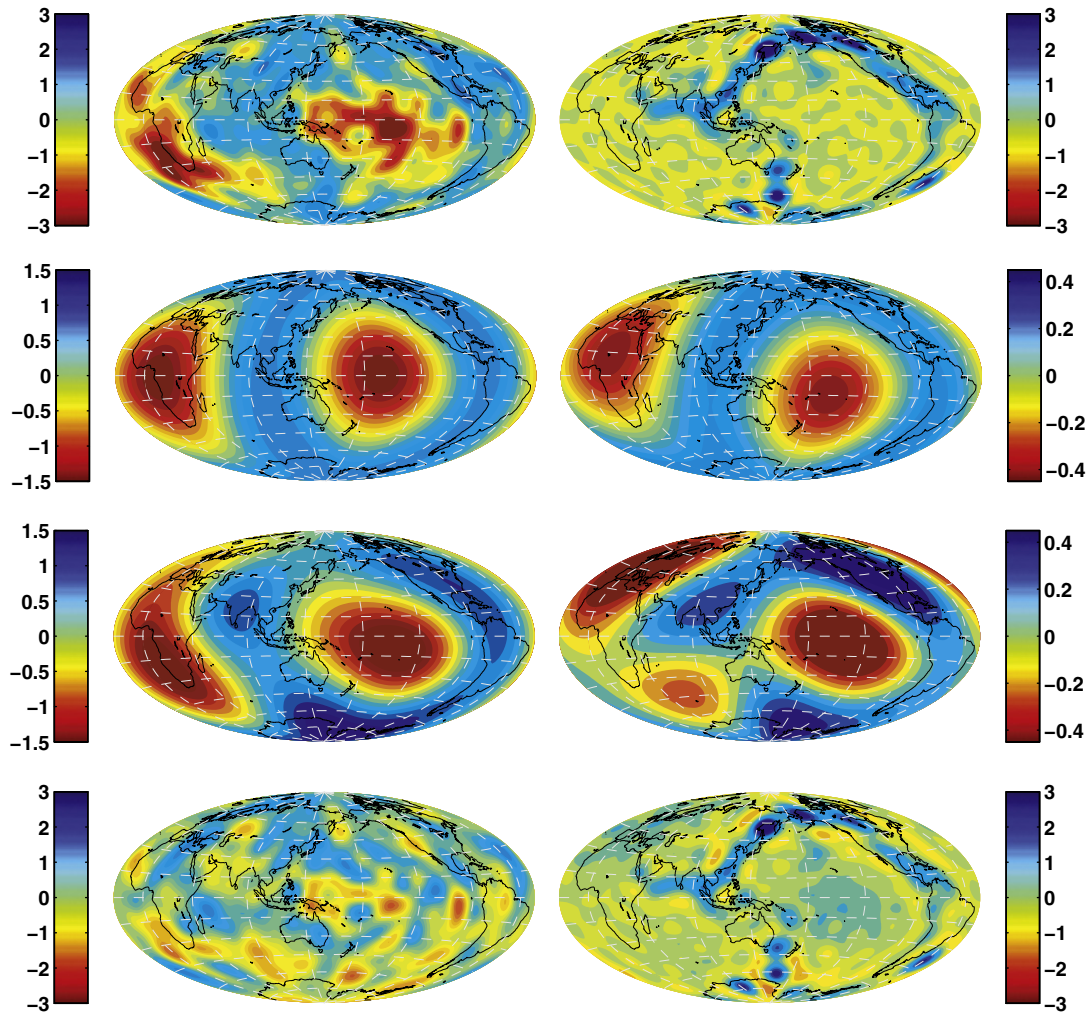
Next, we compare the SLAB110 with the S362ANI velocity anomalies at 2800 km or, effectively, at the CMB. It should be remembered that the information contained in the L-B&R model is derived from surface observations of location of subduction zones and subduction rates during the last 110 Ma; the validity of the 3D density model depends on transforming this information into depth dependence. This may or may not be correct, as we have seen in Figure 5, where comparison with the seismic 3D model indicated that the geometry of the slab flux undergoes major modification in the TZ.

The seismic model (upper left of Fig. 8) shows that velocity anomalies are dominated by two low velocity areas separated by a circum-polar zone of high velocities. The mass anomaly integrated from the slab model, shown in the upper right panel of Figure 8, is represented by a relatively thin ring of positive mass anomalies that, if superimposed on the seismic model, would entirely be within the circum-polar band of higher than average velocities. The rest of the map is flat, as expected. The corresponding power spectra have been shown in Figure 2. The seismic model has a strong peak at degree 2, the power at degree 3 is three times lower and all harmonics higher than 3 have power lower by an order of magnitude than degree 2. For model S362ANI the sum of power contained in degrees 2 and 3 represents about 70% of the power contained in all harmonics from 1 to 18. This can be seen in the center panel of Figure 2, which shows the cumulative power of the models as a function of angular degree. In

contrast, the spectrum of the slab model is rather flat, decreasing slowly from a weak maximum at degree 3 to about 50% at degree 18. Such a spectrum is characteristic of an expansion of linear features on the surface of the sphere (see Fig. 12 in Su and Dziewonski, 1992). The right panel of Figure 2 shows the degree-by-degree correlations of SLAB110 with the same two seismic models as in Figure 5. There is strong correlation for degrees 2 and 3; both seismic models show very similar correlations with SLAB110, which means that our results do not depend strongly on the choice of a particular seismic model.

The second row of Figure 8 compares the degree-2 map of seismic anomalies discussed previously with the degree 2 pattern of SLAB110, integrated over depth. The latter is very similar to that of the seismic model, although the plane of symmetry is slightly tilted with respect to the equator. Whereas the seismic model shows anomalies at 2800 km depth as they exist today, the slab model represents the mass anomaly accumulated within the mantle during the last 110 Ma. Yet, according to L-B&R, they have not yet arrived at the CMB, but the seismic velocity anomalies appear to "anticipate" what is coming. Thus they must represent a record that reaches further than 110 Ma; possibly much further.

Degree 3 is significant both in terms of the power in this degree as well as the high correlation between the seismic and slab model. The third row in Figure 8 shows the velocity anomalies and integrated SLAB110 mass anomalies obtained by combining degree 2 and 3

Fig. 8. *Left column:* Comparison of seismic model S362ANI at 2800 km with the (*right column*) integrated mass anomaly for slab model L-B&R. The top maps show the velocity model at 2800 km and the whole-mantle integrated slab model for degrees 1–18. The second row shows degree-2 pattern only (note the changed color scale), while the third row shows the combined degrees 2 and 3 pattern. The bottom row shows the two models for degrees higher than 3.

coefficients. It is important to remember that in SLAB110 the power in degree 3 is about 4 times larger than in degree 2, when compared to the velocity anomaly model at 2800 km (Fig. 2). These maps show overall similarity, with a correlation coefficient of 0.8 for degree 3, which is significant at the 95% level. The locations of the local extrema are similar but their relative strengths differ. However, because degree 2 is stronger than degree 3 in the seismic model, degree 2 remains dominant, with the influence of degree 3 components imposing a modulation of the details. These include latitudinal elongation of the African Superplume, longitudinal elongation of the Pacific Superplume, three local maxima in the velocities in the fast band: Southeast Asia, North America and Antarctica, and a minimum in the western Indian Ocean. Most of these features exist in the slab model, except that the African superplume has been split in two and the fast band anomalies are substantially stronger. The bottom row in Figure 8 shows the synthesis of harmonics higher than 3. For the seismic model these appear to be random, while for SLAB110 they retain substantial similarity to the complete SLAB110 map (first row, right).

5. Discussion

Strong correlation between the occurrence of the hotspots, geoid, slab subduction and velocity anomalies at the very low degrees (2 and 3) has been shown by Richards and Engebretson (1992). Since that time, until today, the subduction and direct descent of slabs into the lower mantle have been generally thought of as controlling the planform of mantle flow. Note that the highest amplitude large-scale features in the velocity models are negative anomalies. These, of course, do not exist in the slab model, since the mass anomalies in this model are only positive; if this model was complete, the return flow would be very thinly spread over most of the surface of the Earth, so as to preserve the mass balance. Thus, the degree 2 signal in the SLAB110 expansion is determined only by the fast anomalies. But in the map of seismic velocity anomalies, the degree 2 pattern is dictated by both the fast and slow anomalies. The results presented here justify putting forward a different paradigm, namely that the mantle flow is controlled by the degree-2 structure in the deepest 1000 km of the mantle (MAS), with the antipodally located African and Pacific Superplumes being critical, and stable, elements in mantle dynamics.

At degree 2, the axis of the recumbent Y_{20} is centered on the antipodal LLSVPs and also corresponds to the direction of lowest moment of inertia of the Earth, as inferred from the geoid. This indicates an excess of mass along that axis, which could be due to a combination of boundary topography associated with upwellings (e.g. Cazenave et al., 1989) and excess bulk density. Importantly, the integrated mass excess associated with the LLSVPs must dominate over that of the sinking slabs. In the early interpretations of tomographic images, the slow anomalies were associated with higher temperatures, thus the material within the "red" regions was thought to be less dense. In 1997, Su and Dziewonski found that the shear and bulk sound velocity anomalies in the lowermost mantle are anti-correlated; their finding was confirmed by Ishii and Tromp (1999), Kennett et al. (1998) and Masters et al. (2000). This gave a reason to consider compositional variations instead of, or together with, thermal anomalies.

Forte and Mitrovica (2001) considered both thermal and compositional anomalies and concluded that the thermal effects must prevail in order to obtain a satisfactory fit to the geoid. Ishii and Tromp (1999, 2004), whose study is based on interpretation of anomalous splitting of normal modes, suggested that the shear velocity anomalies were also anti-correlated with density. There is some question about our current ability to directly resolve density anomalies in the lower mantle. Regardless of the sign of their density anomaly, superplume density cannot differ from the surrounding mantle by more than 2%, a constraint set by the normal mode analysis of Kuo and Romanowicz

(2002). Kellogg et al. (1999) have proposed that superplumes are neutrally buoyant with the effect of higher temperature within a plume being balanced by higher density; that study—motivated by van der Hilst and Karason's (1999) finding of a compositional heterogeneity in the lowermost 1000 km of the mantle—proposed that there exists a "hot abyssal layer" with a higher concentration of radioactive elements. It could be that the superplumes may be underlain by a material similar to that proposed by Kellogg et al. (1999), in which case, the density of such a layer could be higher, but the overall effect including perturbation in the boundary topography would lead to the result proposed by Forte and Mitrovica (2001).
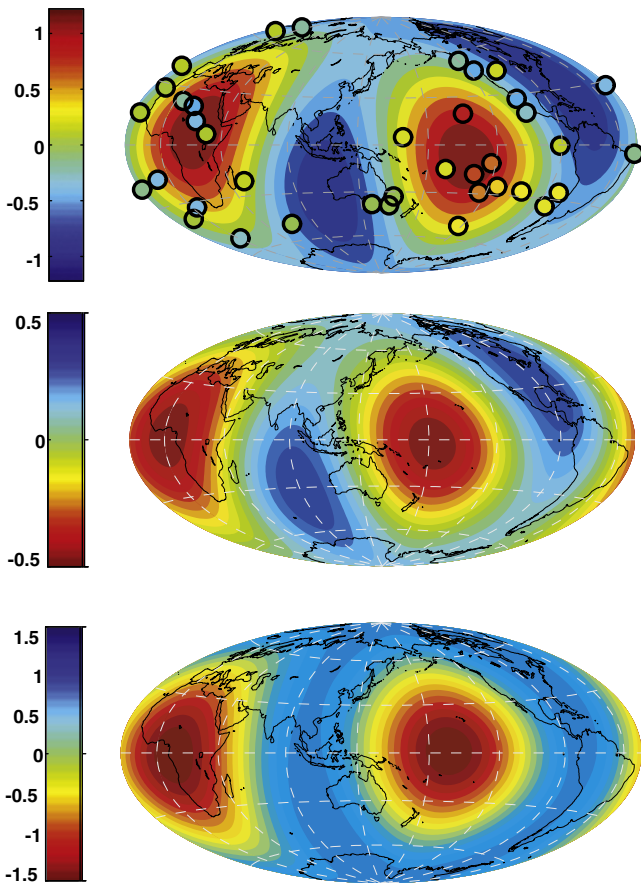
We suggest, on the basis of the probability analysis discussed earlier, that the unique "recumbent" Y_{20} structure—which dominates the deepest 1000 km of the mantle—is long-lived, once it has been established. We do not know when this happened; it could have been early in the history of the Earth: seismology can only tell the present state. It is possible, for example, that in the geological past, owing to some particular initial conditions (e.g. Boyet and Carlson, 2005), mantle convection organized itself in an axi-symmetric planform with a strong quadrupole component (Busse, 1983), to which the axis of rotation adjusted progressively so as to achieve an energetically stable configuration. Once in place, subsequent mass redistribution would have tended to maintain the recumbent Y_{20} configuration, considering that degree 2 is the only one that affects the moment of inertia tensor. The implication is that there is a connection between the development of velocity anomalies and Earth's rotation, with a consequence of long-term stability at the longest wavelengths.

Noting that the SLAB110 model represents slabs that are still sinking in the mantle, while the velocity anomalies near the CMB are already in place, the correlation between the degree 2 in shear velocity in the lowermost mantle and the integrated SLAB110 model has significant implications. Unless there is a major error in the estimation of slab sinking rates, this indicates that the velocity structure near the CMB reflects a combination of processes that took place well before the last 110 Ma.

Another implication of the meridional trend of the "fast zone", which corresponds to the location of subduction zones at the Earth's surface and provides a source of mass redistribution, is that it may be the preferred direction in which true polar wander would occur. As Torsvik et al. (2006) point out, this has, indeed, been the case. In Figure 3, we illustrate the confinement of true polar wander paths within the torus of fast anomalies based on the true polar wander reconstructions of Besse and Courtillot (2002) for the past 200 Ma. The fast torus might be an evolutionary feature that has reached maturity; it might have strengthened and become more even-valued along the polar circle over a long period of accumulation of slab avalanches.

The connection between the location of the superplumes and geologic features at the surface has been noted from the beginning of seismic tomography. For example, Castillo (1988) observed correlation between the low velocities at the CMB in the model of Dziewonski (1984) and occurrence of Dupal anomaly (Dupre and Allegre, 1983), which itself may have been formed early in Earth history (Hart, 1984). As already mentioned, Richards and Engebretson (1992) documented correlation for degrees 2 and 3 between velocity anomalies, location of hot spots, integrated history of subduction and geoid. More recently, Romanowicz and Gung (2002) pointed out the similarity of degree 2 anomalies in velocity at the CMB and attenuation in the transition zone. Figure 9 (top) compares the degree 2 expansion of Steinberger's (2000) hot spots weighted by their mass flux with the attenuation anomalies of Gung and Romanowicz (2004) in the TZ (middle) and with the velocity anomalies of KED at 2800 km depth (bottom). The three maps are very similar, as pointed out by Romanowicz and Gung (2002), supporting their inference that superplumes may heat up the TZ, leading to higher attenuation and to the generation of hotspots. Also, the long-term fixity of hotspots derives naturally from the presence of

Fig. 9. *Top:* distribution of hotspots in compilation of Steinberger (2000), colored by the associated anomalous mass flux (in 10^3 kg/s) in a logarithmic scale. The map shows the degree 2 pattern of this hotspot distribution weighted by each hotspot's anomalous mass flux. *Middle:* the degree 2 pattern of attenuation perturbations at 600 km from the QRLW8 model (Gung and Romanowicz, 2004). *Bottom:* degree 2 pattern of the S-velocity model S362ANI at 2800 km.

stable large-scale upwellings, anchored in the lowermost mantle (Davaille, 1999; Gonnermann et al., 2004; Jellinek and Manga, 2004).

Burke and Torsvik (2004) connected the location of large igneous provinces during the last 200 Ma to the location of the borders of the superplumes, implying that their outline remained unchanged for at least that long; see also Torsvik et al. (2006). Davaille et al. (2005) gave a detailed analysis of the effect of the African Superplume on the history of the break-up of Pangea. Much earlier, Anderson (1982) and Le Pichon and Huchon (1984), Le Pichon et al. (1985) pointed out the geometrical relation between the current geoid pattern and the position of the supercontinent Pangea. While the former favored a top–down control of continental break-up and convergence due simply to thermal insulation by thick continental lithosphere, the latter invoked coupling between upper and lower mantle convection. In our scenario, the geographical fixity of the recumbent Y_{20} would constrain subduction zones to be located within the fast circum-polar band (Fig. 3), away from the two LLSVPs, which, concurrently, would condition spreading, depending on whether oceanic or continental lithosphere was positioned above them at a given time: a supercontinent above one of the LLSVP would lead to thermal blanketing and continental break-up away from the superplume (as observed in the case of Pangea), whereas an oceanic plate above a superplume would experience reduced cooling rate and spread horizontally beyond it before subducting, as currently is the case for the Pacific plate. An important point is that such a scenario, if persistent back into deep geological time, puts strong constraints on continental reconstruc-

tions over multiple past Wilson cycles, and in particular, provides constraints on longitudinal positions that the paleomagnetic record cannot provide. Even though the mechanism proposed was quite different, this was already noted by Anderson (1982).
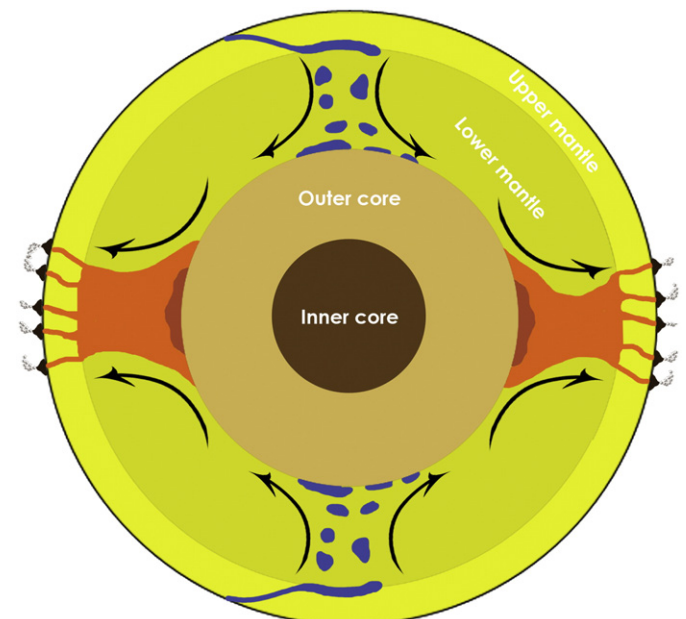
Finally, high correlation between the slab signal for the last 15 Ma and velocity anomalies in the TZ is particularly significant, because we know what happens to subduction until slabs enter the transition zone. The strong degree 2 in the velocity anomalies clearly corresponds to the relatively high recent subduction rate under the western Pacific and South America. The broadening of the velocity anomalies is most simply explained by ponding of the sinking slabs within the TZ as the dominant process; the details of velocity distribution are not inconsistent with an occasional direct slab penetration into the lower mantle; see the map in Figure 1 at 1000 km depth. The difference between fast and slow radial correlation lengths in the lower mantle (Fig. 6) indicates that the fast anomalies may be fragmented, while the slow ones are continuous, which is also confirmed by visual inspection of the models (Fig. 7).

6. Conclusions

Information on the shape of the seismic anomalies in the deepest 1000 km of the mantle has been available for the last quarter of the century. Usually, the anomalies and their significance are considered in the space domain. The most fundamental observation made here is the concentration of power in the "recumbent" Y_{20} anomaly, as shown in Section 3.

Because degree 2 mass anomalies are the only ones that matter for the Earth's moment of inertia tensor, we propose here that the "recumbent" Y_{20} structure, in which the axis of smallest moment of inertia aligns with the LLSVPs, is long-lived, its relative position to the earth's axis of rotation being stable since, possibly, deep geological time. Such a stable configuration would control the planform of mantle convection and the geometry of plate motions at the surface. A recent paper by Torsvik et al. (2010) supports the notion of the superplume stability for the last 200 Ma and possibly 540 Ma. This agrees with our inferences but disagrees with the results of Zhang et al. (2010), whose model predicts a significant change in the strength and location of the African Superplume with time.

We show in Figure 10 a cartoon illustrating the material flux in the mantle, as we envisage it, which agrees, in general, with the

Fig. 10. A cartoon of the equatorial cross-section outlining the proposed circulation in the mantle. Note that the ponded slabs can be partly recirculated in the upper mantle.

mechanism proposed by Romanowicz and Gung (2002). The upward flow of a superplume heats up the bottom of the transition zone. Its higher than average temperature is indicated by the degree-2 pattern of laterally varying attenuation, which correlates well with the velocity anomalies near the CMB. The lower viscosity upper mantle material is then transported to the asthenosphere, where it can spread horizontally, feeding the flow at the spreading centers. Subduction occurs above regions where mantle is relatively cold. The slabs pond in the transition zone; the material may be partially recirculated in the upper mantle and the remainder penetrates into the lower mantle in an avalanche-like process. Some of the former slab material may be entrained in the upward flow created by the hot material in the MAS.

The proposed scenario leaves several challenges and opportunities for other branches of Earth Science to follow up on:

1. The need for geodynamicists to show how a structure such as MAS can develop and why it would remain long-lived, with the exception of minor temporary deviations, such as the small differences of degree 3 anomalies between the slab and velocity models suggests (e.g. Fig. 8c).
2. The need to explain processes in the transition zone: the seismic model clearly shows a behavior characteristic of a boundary layer, although it may be leaky. In general, the connection between the lower and upper mantle must be clarified by additional seismic observations, progress in mineral physics and geodynamic modeling. It is important to constrain the seismic structure by measurements of overtone dispersion (Ritsema et al., 2004). We shall also need higher resolution studies, probably employing seismic broad band arrays to map details of the structure in the transition zone; do plumes originate at the bottom of the transition zone?
3. Our conjecture implies constraints on plate reconstructions beyond the past 200 My. We encourage tectonophysicists to apply these constraints and see if they are compatible with other available data on the motion of continental masses through geological time.
4. The threefold sharp drop in the global r.m.s. velocity perturbations at depths between 200 and 250 km (Fig. 1) indicates that some of the processes above this depth range may be decoupled from the underlying mantle by a low viscosity layer (Becker, 2006). A nearly constant r.m.s. above that depth range implies that this region is not a purely thermal boundary layer; we propose to call it "heterosphere", since—at least for the oceanic structure—it contains both the lithosphere and asthenosphere. This is an additional constraint on geodynamical modeling of convection in the mantle.

References

Anderson, D., 1982. Hotspots, polar wander, Mesozoic convection and the geoid. Nature 297 (5865), 391–393.

Becker, T., Boschi, L., 2002. A comparison of tomographic and geodynamic mantle models. Geochem. Geophys. Geosyst. 3 (1), 1003. doi:10.1029/2001GC000168.

Becker, T., 2006. On the effect of temperature and strain-rate dependent viscosity on global mantle flow, net rotation, and plate-driving forces. Geophys. J. Int. 167 (2), 943–957.

Besse, J., Courtillot, V., 2002. Apparent and true polar wander and the geometry of the geomagnetic field over the last 200 Myr. J. Geophys. Res. 107 (B11), 2300. doi:10.1029/2000JB000050.

Boyet, M., Carlson, R., 2005. 142Nd evidence for early (>4.53 Ga) global differentiation of the silicate Earth. Science 309 (5734), 576–581.

Bull, A., McNamara, A., Ritsema, J., 2009. Synthetic tomography of plume clusters and thermochemical piles. Earth Planet. Sci. Lett. 278 (3–4), 152–162.

Burke, K., Torsvik, T., 2004. Derivation of large igneous provinces of the past 200 million years from long-term heterogeneities in the deep mantle. Earth Planet. Sci. Lett. 227 (3–4), 531–538.

Busse, F., 1983. Quadrupole convection in the lower mantle. Geophys. Res. Lett. 10, 285–288.

Castillo, P., 1988. The Dupal anomaly as a trace of the upwelling lower mantle. Nature 336, 667–670.

Cazenave, A., Souriau, A., Dominh, K., 1989. Global coupling of earth surface topography with hotspots, geoid and mantle heterogeneities. Nature 340, 54–57.

Crough, S.T., Jurdy, D., 1980. Subducted lithosphere, hotspots and the geoid. Earth Planet. Sci. Lett. 48, 15–22.

Davaille, A., 1999. Simultaneous generation of hotspots and superswells by convection in a heterogeneous planetary mantle. Nature 402 (6763), 756–760.

Davaille, A., Stutzmann, E., Silveira, G., Besse, J., Courtillot, V., 2005. Convective patterns under the Indo-Atlantic 'box'. Earth Planet. Sci. Lett. 239 (3–4), 233–252.

Dupre, B., Allegre, C., 1983. Pb–Sr isotope variation in Indian Ocean basalts and mixing phenomena. Nature 303, 142–146.

Dziewonski, A., 1984. Mapping the lower mantle: determination of lateral heterogeneity in P velocity up to degree and order 6. J. Geophys. Res. 89, 5929–5952.

Dziewonski, A., Hager, B., O'Connell, R., 1977. Large-scale heterogeneities in the lower mantle. J. Geophys. Res. 82, 239–255.

Dziewonski, A., Su, W.-J., Woodward, R., 1991. Grand structures of the earth's interior. Eos Transactions, American Geophysical Union, fall meeting supplement 72, 451.

Dziewonski, A., Forte, A., Su, W.-J., Woodward, R., 1993. Seismic tomography and geodynamics. In: Aki, K., Dmowska, R. (Eds.), Relating Geophysical Structures and Processes: The Jeffrey's Volume. : Geophys. Monogr., Vol. 76. American Geophysical Union, pp. 67–105.

Flanagan, M., Shearer, P., 1998. Global mapping of topography on transition zone velocity discontinuities by stacking SS precursors. J. Geophys. Res. 103, 2673–2692.

Foley, B., Becker, T., 2009. Generation of plate-like behavior and mantle heterogeneity from a spherical, viscoplastic convection model. Geochem. Geophys. Geosyst. 10 (8), Q08001.

Forte, A., 2007. Constraints on seismic models from other disciplines—implications for mantle dynamics and composition. In: Romanowicz, B., Dziewonski, A.M. (Eds.), Treatise of Geophysics, Volume 1. Elsevier, pp. 805–858.

Forte, A.M., Mitrovica, J.X., 2001. Deep-mantle high-viscosity flow and thermochemical structure inferred from seismic and geodynamic data. Nature 410, 1049–1056.

Forte, A., Peltier, W., 1987. Plate tectonics and aspherical earth structure: the importance of poloidal–toroidal coupling. J. Geophys. Res. 92, 3645–3680.

Forte, A., Mitrovica, J., Woodward, R., 1995. Seismic-geodynamic determination of the origin of excess ellipticity of the core–mantle boundary. Geophys. Res. Lett. 22 (9), 1013–1016.

Forte, A., Mitrovica, J., Espesset, A., 2002. Geodynamic and seismic constraints on the thermochemical structure and dynamics of convection in the deep mantle. Philos. Trans. R. Soc. Lond. A 360 (1800), 2521–2543.

Fukao, Y., Widiyantoro, S., Bandung, I., Obayashi, M., Tsukuba, J., 2001. Stagnant slabs in the upper and lower mantle transition region. Rev. Geophys. 39, 291–323.

Garnero, E., McNamara, A., 2008. Structure and dynamics of Earth's lower mantle. Science 320 (5876), 626–628.

Goldreich, P., Toomre, A., 1969. Some remarks on polar wandering. J. Geophys. Res. 74, 2555–2567.

Gonnermann, H.M., Mukhopadhyay, S., 2009. Preserving noble gases in a convecting mantle. Nature 459, 560–563.

Gonnermann, H., Jellinek, A., Richards, M., Manga, M., 2004. Modulation of mantle plumes and heat flow at the core mantle boundary by plate-scale flow: results from laboratory experiments. Earth Planet. Sci. Lett. 226 (1–2), 53–67.

Grand, S., van der Hilst, R.D., Widiyantoro, S., 1997. Global seismic tomography: a snapshot of convection in the Earth. GSA Today 7 (4), 1–7.

Gu, Y., Dziewonski, A., Su, W., Ekstrom, G., 2001. Models of the mantle shear velocity and discontinuities in the pattern of lateral heterogeneities. J. Geophys. Res. 106 (B6), 11,169–11,199.

Gu, Y.J., Dziewonski, A.M., Ekstrom, G., 2003. Simultaneous inversion for mantle shear velocity and topography of transition zone discontinuities. Geophys. J. Int. 154, 559–583.

Gung, Y., Romanowicz, B., 2004. Q tomography of the upper mantle using three-component long-period waveforms. Geophys. J. Int. 157, 813–830. doi:10.1111/j.1365-246X.2004.02265.x.

Hager, B., 1984. Subducted slabs and the geoid—constraints on mantle rheology and flow. J. Geophys. Res. 89 (B7), 6003–6015.

Hart, S., 1984. A large-scale isotope anomaly in the Southern Hemisphere. Nature 309, 753–756.

Hartlep, T., Tilgner, A., Busse, F., 2003. Large scale structures in Rayleigh–Benard convection at high Rayleigh numbers. Phys. Rev. Lett. 91 (6), 64501.

Ishii, M., Tromp, J., 1999. Normal-mode and free-air gravity constraints on lateral variations in velocity and density of earth's mantle. Science 285, 1231–1236.

Ishii, M., Tromp, J., 2004. Constraining large-scale mantle heterogeneity using mantle and inner-core sensitive normal modes. Phys. Earth Planet. Inter. 146 (1–2), 113–124.

Jellinek, A., Manga, M., 2004. Links between long-lived hot spots, mantle plumes, D″, and plate tectonics. Rev. Geophys. 42 (RG3002). doi:10.1029/2003RG000144.

Jordan, T., Puster, P., Glatzmaier, G., Tackley, P., 1993. Comparisons between seismic Earth structures and mantle flow models based on radial correlation functions. Science 261 (5127), 1427–1431.

Kellogg, L., Hager, B., van der Hilst, R., 1999. Compositional stratification in the deep mantle. Science 283 (5409), 1881–1884.

Kennett, B.L.N., Widiyantoro, S., van der Hilst, R., 1998. Joint seismic tomography for bulk sound and shear wave speed in the Earth's mantle. J. Geophys. Res. 103, 12,469–12,493.

Kuo, C., Romanowicz, B., 2002. On the resolution of density anomalies in the earth mantle using spectral fitting of normal mode data. Geophys. J. Int. 150, 162–179.

Kustowski, B., 2007. Modeling the anisotropic shear-wave velocity structure in the earths mantle on global and regional scales. Ph.D. thesis, Harvard University.

Kustowski, B., Ekstrom, G., Dziewonski, A.M., 2008. Anisotropic shear-wave velocity structure of the earth's mantle: a global model. J. Geophys. Res. 113 (B12), 806306. doi:10.1029/2007JB005169.

Lay, T., 2007. Deep earth structure—lower mantle and D″. In: Romanowicz, B., Dziewonski, A. (Eds.), Treatise on Geophysics. : Seismology and Structure of the Earth, Vol. 1. Elsevier.

Le Pichon, X., Huchon, P., 1984. Geoid, Pangea and convection. Earth Planet. Sci. Lett. 67, 123–135.

Le Pichon, X., Huchon, P., Barrier, E., 1985. Pangea, geoid and the evolution of the western margin of the Pacific Ocean. In: Nasa, N., et al. (Ed.), Formation of Active Ocean Margins, pp. 3–42.

Lekic, V., 2004. Distribution of stresses in descending lithospheric slabs from a global survey of Harvard CMT solutions for subduction-zone earthquakes. Honor's Thesis, Harvard University.

Lithgow-Bertelloni, C., Richards, M., 1998. The dynamics of Cenozoic and Mesozoic plate motions. Rev. Geophys. 36 (1), 27–78.

Lundgren, P., Giardini, D., 1994. Isolated deep earthquakes and the fate of subduction in the mantle. J. Geophys. Res. Solid Earth 99 (B8), 15833–15842.

MacDonald, G.J.F., 1965. The figure and long-term mechanical properties of the Earth. In: Hurley, P.M. (Ed.), Advances in Earth Science, pp. 199–245.

Machetel, P., Weber, P., 1991. Intermittent layered convection in a model mantle with an endothermic phase change at 670 km. Nature 350, 55–57.

Masters, G., Jordan, T., Silver, P., Gilbert, F., 1982. Aspherical Earth structure from fundamental spheroidal-mode data. Nature 298, 609–613.

Masters, G., Laske, G., Bolton, H., Dziewonski, A., 2000. The relative behavior of shear velocity, bulk sound speed, and compressional velocity in the mantle: implications for chemical and thermal structure. In: Karato, S., Forte, A.M., Liebermann, R.C., Masters, G., Stixrude, L. (Eds.), Earth's Deep Interior: Mineral Physics and Tomography from Atomic to the Global Scale. AGU, Washington D.C, pp. 63–87.

McKenzie, D.P., 1966. The viscosity of the lower mantle. J. Geophys. Res. 71, 3995–4010.

Megnin, C., Romanowicz, B., 2000. The three-dimensional shear velocity structure of the mantle from the inversion of body, surface and higher mode waveforms. Geophys. J. Int. 143, 709–728.

Morgan, W., 1972. Deep mantle convection plumes and plate motions. Am. Assoc. Pet. Geol. Bull. 56 (2), 203–213.

Panning, M., Romanowicz, B., 2006. A three-dimensional radially anisotropic model of shear velocity in the whole mantle. Geophys. J. Int. 167, 361–379.

Pysklywec, R., Mitrovica, J., Ishii, M., 2003. Mantle avalanche as a driving force for tectonic reorganization in the southwest Pacific. Earth Planet. Sci. Lett. 209 (1–2), 29–38.

Ricard, Y., Richards, M., Lithgow-Bertelloni, C., Stun_, Y.L., 1993. A geodynamic model of mantle density heterogeneity. J. Geophys. Res. 98, 21895–21910.

Richards, M., Engebretson, D., 1992. Large-scale mantle convection and the history of subduction. Nature 355, 437–440.

Richards, M.A., Hager, B.H., 1984. Geoid anomalies in a dynamic earth. J. Geophys. Res. 89, 5987–6002.

Ritsema, J., Heijst, H., Woodhouse, J., 1999. Complex shear wave velocity structure imaged beneath Africa and Iceland. Science 286 (5446), 1925–1928.

Ritsema, J., van Heijst, H.J., Woodhouse, J.H., 2004. Global transition zone tomography. J. Geophys. Res. 109 (B02302). doi:10.1029/2003JB002610.

Romanowicz, B., Gung, Y., 2002. Superplumes from the core–mantle boundary to the lithosphere: implications for heat flux. Science 296 (5567), 513–516.

Solheim, L., Peltier, W., 1994. Avalanche effects in phase transition modulated thermal convection: a model of Earth's mantle. J. Geophys. Res. 99 (B4), 6997–7018.

Steinberger, B., 2000. Plumes in a convecting mantle: models and observations for individual hotspots. J. Geophys. Res. 105 (B5), 11127–11152.

Steinberger, B., O'Connell, R., 1997. Changes of the Earth's rotation axis owing to advection of mantle density heterogeneities. Nature 387 (6629), 169–173.

Steinberger, B., Torsvik, T.H., 2008. Absolute plate motions and true polar wander in the absence of hotspot tracks. Nature 452, 620–623.

Su, W., Dziewonski, A.M., 1992. On the scale of mantle heterogeneity. Phys. Earth Planet. Inter. 74, 29–54.

Su, W.-J., Dziewonski, A.M., 1997. Simultaneous inversions for 3-D variations in shear and bulk velocity in the mantle. Phys. Earth Planet. Inter. 100, 135–156.

Tackley, P., Stevenson, D., Glatzmaier, G., Schubert, G., 1993. Effects of an endothermic phase transition at 670 km depth in a spherical model of convection in the Earth's mantle. Nature 361 (6414), 699–704.

Tackley, P., Stevenson, D., Glatzmaier, G., Schubert, G., 1994. Effects of multiple phase transitions in a three-dimensional spherical model of convection in Earth's mantle. J. Geophys. Res. 99, 15877–15901.

Torsvik, T., Smethurst, M., Burke, K., Steinberger, B., 2006. Large igneous provinces generated from the margins of the large low-velocity provinces in the deep mantle. Geophys. J. Int. 167 (3), 1447–1460.

Torsvik, T., Burke, K., Steinberger, B., Webb, S.J., Ashwal, L.D., 2010. Diamonds sampled by plumes from the core–mantle boundary. Nature 466, 352–356.

van der Hilst, R., Karason, H., 1999. Compositional heterogeneity in the bottom 1000 kilometers of the Earth's mantle: toward a hybrid convection model. Science 283 (5409), 1885–1888.

van der Hilst, R., Widiyantoro, S., Engdahl, E., 1997. Evidence for deep mantle circulation from global tomography. Nature 386 (6625), 578–584.

van der Hist, R., Engdahl, R., Spakman, W., Nolet, G., 1991. Tomographic imaging of subducted lithosphere below northwest Pacific island arcs. Nature 353 (6339), 37–43.

Woodhouse, J.H., Dziewonski, A.M., 1984. Mapping the upper mantle: three dimensional modeling of earth structure by inversion of seismic waveforms. J. Geophys. Res. 89, 5953–5986.

Woodward, R.L., Dziewonski, A.M., Peltier, W.R., 1994. Comparisons of seismic heterogeneity models and convective flow calculations. Geophys. Res. Lett. 21, 325–328.

Zhang, N., Zhong, S., Leng, W., Li, Z.-X., 2010. A model for the evolution of the Earth's mantle structure since the Early Paleozoic. J. Geophys. Res. 115, B06401. doi:10.1029/2009JB006896.

Zhong, S., Zhang, N., Li, Z., Roberts, J., 2007. Supercontinent cycles, true polar wander, and very long-wavelength mantle convection. Earth Planet. Sci. Lett. 261 (3–4), 551–564.